Binary Kinetics in the Y–Ba–Cu System: 1. Mixed Powders

Jeffrey L. Sobolik and William J. Thomson
Dept. of Chemical Engineering, Washington State University, Pullman, WA 99164

The kinetics of the reactions between mixed powders of $BaCO_3$ and CuO, as well as $BaCO_3$ and Y_2O_3, have been studied using DXRD techniques as a function of particle size, temperature, and CO_2 pressure. Except for initial nucleation phenomena, the reaction rates are governed by shrinking core behavior for $BaCO_3$ particle sizes between 6 and 33 μm. During the initial stages of the reactions, the surface reaction kinetics are governing, whereas the diffusion of CuO, Y_2O_3, and CO_2 are limiting factors at later stages in the reactions. Quantitative conversion data were used to determine the values of the activation energies and the pertinent diffusivities in these systems.

Introduction

With the advent of large-scale processing of ceramic powders, particularly those that are synthesized on a nanosize scale, interest in the kinetics of solid–solid reactions has grown. Tamhankar and Doraiswamy (1979) have reviewed the state of information on this subject as of 1979, but progress has been slow. One of the difficulties is the lack of a phase-specific probe capable of following the extent of solid–solid reactions in real time. The relatively recent development of time-resolved X-ray diffraction, particularly dynamic X-ray diffraction (DXRD) (Thomson, 1989), now affords an unambiguous experimental technique for quantitative studies of the rates of solid–solid reactions. A good example of a solid-state reacting system in need of a systematic kinetic study is the Y–Ba–Cu high-temperature superconductor (123 HTSC). Since good superconducting properties are highly dependent on the ability to obtain a phase-pure product, a knowledge of the governing kinetics under processing conditions would be highly desirable.

Due to the lack of detailed knowledge about the solid-state reaction mechanism leading to the formation of the 123 HTSC, many different sintering processes have been used in different laboratories. In one study (Jiang et al., 1988) using differential thermal analysis (DTA), thermogravimetric analysis (TGA), and X-ray diffraction (XRD), mixed powders of Y_2O_3, $BaCO_3$, and CuO were sintered to produce the tetragonal 123 phase. Although the particle size of the powders was not given, the reaction leading to the final product was initiated at about 1,073 K in air and consisted of the formation of barium cuprate by

$$BaCO_3 + CuO \rightleftharpoons BaCuO_2 + CO_2, \quad (1)$$

which then reacted with the oxides of yttrium and copper from 1,073–1,203 K to give

$$Y_2O_3 + 4BaCuO_2 + 2CuO \rightleftharpoons 2YBa_2Cu_3O_6 + \frac{1}{2}O_2 \quad (2)$$

They concluded that during the sintering process, $BaCuO_2$ formed prior to the 123 phase and promoted the decomposition of $BaCO_3$, but also became the primary source of undesirable phases in the 123 HTSC if it remained unreacted due to unsuitable heat treatment. The two-step process was determined to be controlled by a second-order chemical reaction and had an activation energy of about 192 kJ/mol. The effect of the gaseous environment on the reaction was also studied, and the results showed that the reaction temperatures were reduced by 100 K when the system was sintered in an oxygen-free environment.

Because the presence of $BaCO_3$ was originally thought to hinder the rapid formation of the 123 HTSC due to its low decomposition rate at temperatures between 1,173 and 1,223 K, Ruckenstein and Wu (1988) conducted a study in an attempt to avoid this apparent rate-limiting step. They found that reaction rates could be increased if $BaCO_3$ and CuO were first reacted to form $BaCuO_2$, which was subsequently

Correspondence concerning this article should be addressed to W. J. Thomson. Present address of J. L. Sobolik: Battelle PNL, Richland, WA 99352.

reacted with Y_2O_3 and CuO to form the 123 HTSC in air, consistent with the reaction scheme given in Eqs. 1 and 2. Furthermore, the particle size of the $BaCuO_2$ product was classified with sedimentation techniques to show the dependence of the reaction rate on the particle size of the starting materials. By using the classified $BaCuO_2$ particles, the tetragonal phase of the 123 superconductor formed at 1,203 K in less than 2 h and had a narrow particle-size distribution (~ 1–1.5 μm) compared to the broad particle-size distribution (~ 1–20 μm) that was obtained when the unclassified ternary mixture was sintered for 20 h. Unfortunately, the authors did not report on the particle sizes of their precursors other than to mention that the reactants agglomerated, resulting in heterogeneous products as a consequence of macroscopic diffusion limitations present in the ~ 100-g samples used. Furthermore, the bulk density and T_c of the final product were found to increase when the calcination times were shortened.

In a follow-up study (Ruckenstein et al., 1989), the combination reactions of Y_2O_3, $BaCO_3$, BaO, CuO, $BaCuO_2$, and $Y_2Cu_2O_5$ were analyzed using XRD on air-quenched samples (~ 0.5 g) calcined at 1,213 K in air for various time intervals. Two reaction pathways were suggested as being most efficient: (a) preparation of $BaCuO_2$ in a first step followed by its reaction with $Y_2Cu_2O_5$ in a second step; (b) preparation of $BaCuO_2$ in a first step followed by its reaction with CuO and Y_2O_3 in a second step. In the latter case, however, the intermediate compounds of Y_2BaCuO_5 (211) and $Y_2Cu_2O_5$ were present in larger amounts than when $BaCuO_2$ and $Y_2Cu_2O_5$ were employed to prepare the superconducting compound. It was proposed that when the ternary mixture of $BaCuO_2$, Y_2O_3, and CuO was used, trace amounts of 211 and $Y_2Cu_2O_5$, undetectable by XRD, may have been present and unable to react even after long calcination times, thus affecting the critical current density of the final product. It was concluded that the decomposition of $BaCO_3$ was the major limiting factor in both cases, and it was suggested that in order to achieve a high-density product, the particle size of the $BaCO_3$ should be as small as possible and the particle-size distribution should be sufficiently narrow.

Gadalla and Hegg (1989) used TGA and DTA to study the reaction kinetics of the ternary mixture (~ 0.12 g) of $BaCO_3$, CuO, and Y_2O_3. The reaction was carried out in an air environment, and the particle sizes of the starting materials were not given. To determine the intermediate phases appearing during the formation of the 123 compound, the constituents were mixed, fired at different temperatures for different periods of time, and examined by X-ray diffraction (air-quenched). They concluded that the 123 HTSC formed by the reaction of the two intermediates, $BaCuO_2$ and (211). By using dynamic analysis methods, which is the determination of the degree of transformation as a function of time during a linear increase of temperature, they were able to conclude that the reaction was diffusion controlled but did not specify the controlling species. Finally, the activation energies of their six-step process ranged from 40 to 800 kJ/mol.

Since the particle size of the starting materials was considered to greatly influence the overall formation reaction of the 123 HTSC, Huang et al. (1989) made use of differential scanning calorimetry (DSC) and TGA to study particle-size effects. Ternary mixtures (~ 0.4 g) of various cationic stoichiometric ratios of Y_2O_3, $BaCO_3$, and CuO with particle sizes ranging from 0.5 to 8 microns were used in their study. XRD on interrupted, air-quenched specimens indicated that the 123 HTSC formed from two consecutive and overlapping steps during continuous heating; the reaction of previously formed $BaCuO_2$ with Y_2O_3 and CuO as well as the reaction of previously formed Ba_2CuO_3 with Y_2O_3 and CuO. The two steps had activation energies of 502 and 753 kJ/mol, respectively. All of the experiments were conducted in air and when the average particle size was reduced from 8 to 0.5 microns, the optimum isothermal temperature for forming the 123 HTSC phase was lowered from 1,200 to 1,163 K.

Finally, Wu et al. (1990) studied the single reaction, $Y_2BaCuO_5 + 3BaCuO_2 + 2CuO \rightarrow 2YBa_2Cu_3O_{6.5-x} + xO_2$, using TGA and XRD. The reaction of the calcined powders (~ 100 g samples) was carried out in air and, by fitting the data to their developed model, it was established that the reaction was controlled by the diffusion of Ba^{+2} and was best described by a three-dimensional diffusion mechanism containing a particle-size dependence. However, the experiments were only conducted with powders of one average particle size (3 μm), so the validity of the model could not be tested. The activation energy was determined to be 2,176 kJ/mol.

In a previous study (Sobolik et al., 1993), the reaction pathways leading to the formation of the $YBa_2Cu_3O_{6.5}$ high-T_c superconductor (123 HTSC) were observed using DXRD (Thomson et al., 1989). The effect of particle size and the gaseous environment on the binary reaction paths of the three precursors Y_2O_3, $BaCO_3$, and CuO were observed but not quantified. The use of DXRD avoided the necessity of quenching or indirect measurements such as mass or enthalpy changes, thereby providing unambiguous observations of each of the crystalline transformations as they occur. By using this technique, all reaction intermediates, temperatures, and environments were readily observed. The results showed that when the particle size of the precursors was reduced from 6–10 μm to 6–120 nm in conjunction with the amount of oxygen and carbon dioxide present, the temperature requirements necessary to favor reaction products were reduced by 20 to 150 K. Furthermore, in both air and helium environments, the only observed reaction in the nanometer-sized system leading to the formation of the 123 HTSC was

$$Y_2O_3 + 4BaCO_3 + 6CuO \rightleftharpoons 2Y_2Ba_3Cu_3O_{6.5} + 4CO_2 \quad (3)$$

In the mixture containing the larger particles, however, barium- and copper-containing compounds were also observed, with the major intermediate being $BaCuO_2$, which formed by Eq. 1. Since the reaction temperatures necessary to form the 123 HTSC by Eq. 3 were very similar to those required to form $BaCuO_2$ by Eq. 1, it is likely that $BaCuO_2$ is a species that is very influential in determining the quality of the final 123 HTSC product.

When $BaCO_3$ reacts according to Eqs. 1 and 3, CO_2 is released and becomes locally concentrated near its equilibrium value. These stagnant regions of CO_2 can inhibit the progress of Eqs. 1 and 3 as well as cause the decomposition reaction of the 123 HTSC (the reverse of Eq. 3) that produces undesirable phases that ultimately contribute to the reduction of the critical current density of the final product (Fjellvåg et al., 1988; Gao et al., 1990; Cooper et al., 1991;

Selvaduray et al., 1992). Ideally, when a better understanding of the events leading to these alterations is achieved, corrective steps can be taken during processing to improve the quality of the final product.

In light of the work of others, it becomes evident that the partial pressure of CO_2 within the reacting system and the particle size of $BaCO_3$ have a major impact on the rate limitations that hinder rapid formation of the 123 HTSC. Since the reaction between $BaCO_3$ and CuO plays a major role in the processing of the 123 HTSC, a study that delineates the mechanism that controls Eq. 1 is necessary. In order to assess the effect of particle size on the *rates* of Eq. 1, this study was conducted using $BaCO_3$ with three different particle sizes (6.2, 14, and 33 μm). Furthermore, the reaction study was conducted isothermally (1,083–1,153 K) in different partial pressures of CO_2 (0.03–0.27 kPa). Finally, these same particle sizes of $BaCO_3$ were reacted with Y_2O_3 under similar conditions in order to compare the characteristics of the two systems since the $BaCO_3$:CuO reaction is common to the processing of the 123 HTSC while the Y_2O_3:$BaCO_3$ reaction is not.

Theoretical Development

The reaction of carbonates is an equilibrium process controlled by the CO_2 partial pressure at the reaction interface (Campbell, 1978). The mechanism for the reaction of carbonates is initiated by a formation of nuclei within the crystal lattice sites, followed by the growth of the nuclei across the surface and interior of the crystal. The simplest kinetic scheme results when the nucleation and surface growth are fast, and therefore the rate of reaction is determined by the progression of the reaction front into the particle (Figure 1). Based on this information, one can write the rate of reaction for Eq. 1 as

$$-\frac{dN_{BaCO_3}}{dt} = k_f a_{BaCo_3} a_{CuO} - k_r a_{BaCuO_2} P_{CO_2} \qquad (4)$$

where k_f and k_r are the forward and reverse rate constants, respectively; $a_{(i)}$ is the activity of each phase present; and P_{CO_2} is the partial pressure of CO_2 at the reaction front. By assuming that the activity of the mobile phase, CuO, is proportional to its concentration at the reaction surface, Eq. 4 can be rearranged to give

$$-\frac{dN_{BaCO_3}}{dt} = k_f a_{BaCO_3} k_{CuO} C_{CuO}\left[1 - \frac{k_r a_{BaCuO_2} P_{CO_2}}{k_f a_{BaCO_3} k_{CuO} C_{CuO}}\right]. \qquad (5)$$

At equilibrium

$$\frac{k_r a_{BaCuO_2} P^{eq}_{CO_2}}{k_f a_{BaCO_3} k_{CuO} C_{CuO}} = 1, \qquad (6)$$

and assuming that the activity of $BaCO_3$ is proportional to the surface area at the $BaCO_3$–$BaCuO_2$ interface, Eq. 6 becomes

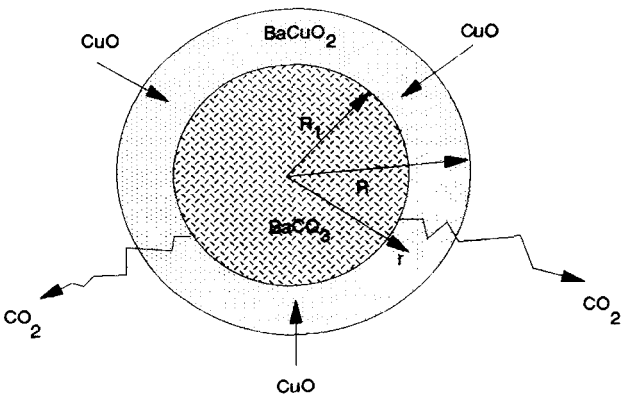

Figure 1. Reaction sphere.

$$-\frac{dN_{BaCO_3}}{dt} = k' 4\pi R_1^2 C_{CuO}\left[1 - \frac{P_{CO_2}}{P^{eq}_{CO_2}}\right] \qquad (7)$$

where $k_1 = k_f k_{BaCO_3} k_{CuO}$ and C_{CuO} and P_{CO_2} are the values at the reaction interface, that is, at R_1.

To confirm the assumptions that $BaCO_3$ and $BaCuO_3$ were the stationary phases while the CuO was the mobile phase responsible for diffusing through the product layer, an electron beam line scan was conducted on a partially reacted 33-μm $BaCO_3$ particle with a Cameca Electron Micro-Probe, and the resulting backscatter electron image is shown in Figure 2. Figure 2a shows the scan of the elemental Ba and demonstrates that barium is present throughout the entire body of the particle. Figure 2b, however, shows the scan of elemental Cu and demonstrates that copper is present only on the outer edge of the particle, which confirms our assumption that the copper diffuses through the stationary $BaCuO_2$ product to react with the $BaCO_3$ core.

The rate of Eq. 1 may also be controlled by the rate of diffusion of CuO to the reaction front as well as the rate of diffusion of CO_2 away from the reaction front as shown in Figure 1. Diffusion-controlled solid-state reactions occur when these resistances to diffusion through the product layer control the rate of reaction. The steps leading to an expression between time and dimension are twofold (Levenspiel, 1972). Initially, a relationship for the flux is obtained for a particle that has partially reacted, assuming quasi-steady-state conditions. This relationship for the reaction flux is used to determine the rate of disappearance of the unreacted core and is integrated over time to obtain an expression for $R_1(t)$.

In deriving the mechanism that takes the diffusion of both CuO and CO_2 into account, CuO is considered to move inward toward the unreacted core and CO_2 migrates outward from the reaction front. But the progression of the reaction front is much slower than the flow rates of CuO and CO_2 to and from the unreacted core, respectively (the system is under "quasi-steady-state" conditions). Because of this, it is assumed, in considering the concentration gradients of each species in the product layer at any time, that the unreacted core is stationary. By using this assumption, the rates of reaction of CuO and CO_2 at any instant in time are given by their respective rates of diffusion to and from the reaction front, or

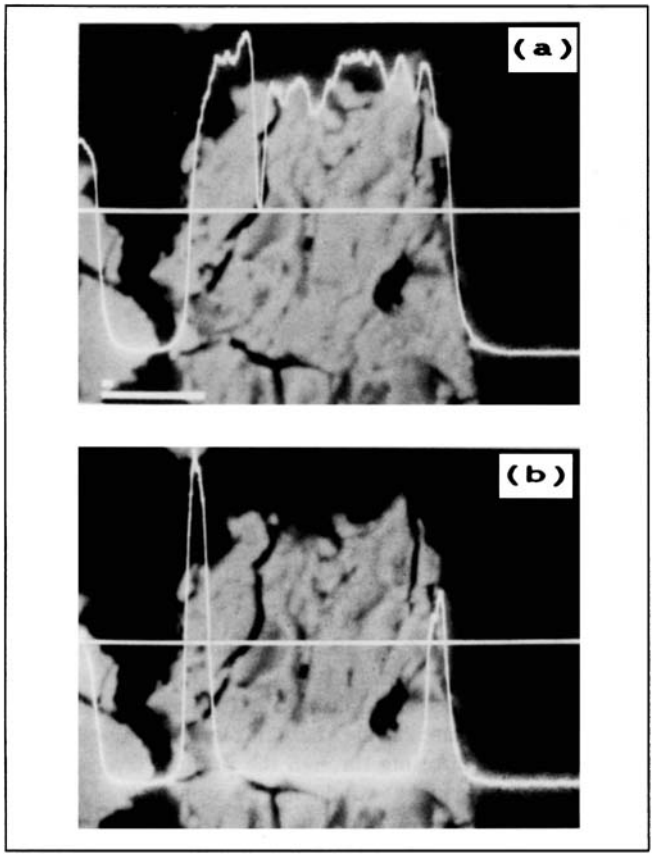

Figure 2. Electron beam line scan on a partially reacted 33-μm particle.
(a) Elemental Ba. (b) Elemental Cu.

$$-\frac{dN_{BaCO_3}}{dt}=-\frac{dN_{CuO}}{dt}=4\pi R_1^2\left(D_{CuO}\frac{dC_{CuO}}{dr}\right)_{|R_1} \tag{8}$$

and

$$-\frac{dN_{BaCO_3}}{dt}=\frac{dN_{CO_2}}{dt}=4\pi R_1^2\left(-D_{CO_2}\frac{dC_{CO_2}}{dr}\right)_{|R_1} \tag{9}$$

where $D_{(i)}$ are the diffusion coefficients of each species.

To solve Eq. 7, expressions for C_{CuO} and P_{CO_2} as functions of r must first be obtained. This can be achieved by performing a mass balance on both species in the product layer: $R_1 \le r \le R$. For CuO, we have

$$\frac{d}{dr}r^2D_{CuO}\frac{dC_{CuO}}{dr}=0 \tag{10}$$

with the boundary condition at $r = R$,

$$C_{CuO}=C_{CuO}^{bulk}. \tag{11}$$

Equating Eqs. 7 and 8 at $r = R_1$, the secondary boundary condition can be obtained from

$$D_{CuO}\frac{dC_{CuO}}{dr}|_{R_1}=k_1'C_{CuO_{|R_1}}\left[1-\frac{P_{CO_{2|R1}}}{P_{CO_2}^{eq}}\right]. \tag{12}$$

When Eq. 10 is solved with the boundary conditions Eqs. 11 and 12, an expression for $C_{CuO}(r)$ is obtained

$$C_{CuO}(r)=C_{CuO}^{bulk}-\frac{k_1'C_{CuO_{|R_1}}R_1^2}{D_{CuO}}\left[1-\frac{P_{CO_{2|R1}}}{P_{CO_2}^{eq}}\right]\left[\frac{1}{r}-\frac{1}{R}\right]. \tag{13}$$

Similarly, the mass balance for CO_2 in the product layer yields

$$\frac{d}{dr}r^2D_{CO_2}\frac{dP_{CO_2}}{dr}=0 \tag{14}$$

with the boundary condition at $r = R$,

$$P_{CO_2}=P_{CO_2}^{bulk}, \tag{15}$$

and at $r = R_1$, equating Eqs. 7 and 9 while using the ideal gas law gives

$$-D_{CO_2}\frac{dP_{CO_2}}{dr}|_{R_1}=k_1'(R_gT)C_{CuO_{|R_1}}\left[1-\frac{P_{CO_{2|R1}}}{P_{CO_2}^{eq}}\right] \tag{16}$$

where R_g is the ideal gas constant and T is the temperature, which is assumed to be equal to the bulk temperature. When Eq. 14 is solved with the boundary conditions, Eqs. 15 and 16, an expression for $P_{CO_2}(r)$ is obtained

$$P_{CO_2}(r)=P_{CO_2}^{bulk}+\frac{k_1'(R_gT)C_{CuO_{|R_1}}R_1^2}{D_{CO_2}}\left[1-\frac{P_{CO_{2|R1}}}{P_{CO_2}^{eq}}\right]\left[\frac{1}{r}-\frac{1}{R}\right]. \tag{17}$$

The next step in obtaining the model involves evaluating Eqs. 13 and 17 at the reaction surface at R_1, and placing the resulting expressions into Eq. 7. Variations of R_1 with time can be obtained from a mass balance on the unreacted core

$$\frac{dN_{BaCO_3}}{dt}=\frac{d}{dt}\left[\rho_{BaCO_3}\frac{4}{3}\pi R_1^3\right] \tag{18}$$

so that Eq. 7 becomes

$$-\frac{dR_1}{dt}=\frac{k_1'C_{CuO_{|R_1}}}{\rho_{BaCO_3}}\left[1-\frac{P_{CO_{2|R1}}}{P_{CO_2}^{eq}}\right]. \tag{19}$$

We can integrate Eq. 19 and solve for $R_1(t)$ provided we have expressions for $P_{CO_{2|R1}}$ and $C_{CuO_{|R_1}}$. The approach is to independently assume that diffusion gradients are negligible for CO_2 and then for CuO. In the former case, $P_{CO_{2|R1}} \approx P_{CO_2}^{bulk}$, and Eq. 13 can be solved for $C_{CuO_{|R_1}}$ and, in the latter,

$C_{CuO_{|R_1}} = C_{CuO}^{bulk}$ and Eq. 17 can be solved for $P_{CO_{2|R1}}$. This yields

Negligible CO_2 Gradients

$$-\left[P_{CO_2}^{eq} - \frac{k_1}{D_{CuO}}\left(P_{CO_2}^{eq} - P_{CO_2}^{bulk}\right)\left(\frac{R_1^2}{R} - R\right)\right]dR_1 = \frac{k_1' C_{CuO}^{bulk}}{\rho_{BaCO_3}}\left[P_{CO_2}^{eq} - P_{CO_2}^{bulk}\right]dt. \quad (20)$$

Negligible CuO Gradients

$$-\left[P_{CO_2}^{eq} + \frac{k_1' R_g T C_{CuO}^{bulk}}{D_{CO_2}}\left(R_1 - \frac{R_1^2}{R}\right)\right]dR_1 = \frac{k_1' C_{CuO}^{bulk}}{\rho_{BaCO_3}}\left[P_{CO_2}^{eq} - P_{CO_2}^{bulk}\right]dt. \quad (21)$$

Since the two resistances due to CuO and CO_2 given in Eqs. 20 and 21 act simultaneously, the time required to reach any stage of conversion is equal to the sum of the times needed if each resistance acted alone (Levenspiel, 1972), or

$$t_{total} = t_{CuO\ alone} + t_{CO_2\ alone}. \quad (22)$$

With this in mind, Eqs. 20 and 21 can be combined to give

$$-\int_R^{R_1}\left[2P_{CO_2}^{eq} + k_1'\left[\frac{R_g T C_{CuO}^{bulk}}{D_{CO_2}} + \frac{P_{CO_2}^{eq} - P_{CO_2}^{bulk}}{D_{CuO}}\right] \times\left(R_1 - \frac{R_1^2}{R}\right)\right]dR_1 = \frac{k_1' C_{CuO}^{bulk}}{\rho_{BaCO_3}}\left[P_{CO_2}^{eq} - P_{CO_2}^{bulk}\right]\int_0^t dt, \quad (23)$$

which can be integrated in terms of fractional conversion, α, by noting that $(R_1/R)^3 = (1-\alpha)$, to give

$$\frac{12P_{CO_2}^{eq}}{R}[1-(1-\alpha)^{1/3}] + k_1'\left[\frac{R_g T C_{CuO}^{bulk}}{D_{CO_2}} + \frac{P_{CO_2}^{eq} - P_{CO_2}^{bulk}}{D_{CuO}}\right][1-3(1-\alpha)^{2/3}+2(1-\alpha)] = \frac{6k_1' C_{CuO}^{bulk}}{R^2\rho_{BaCO_3}}\left[P_{CO_2}^{eq} - P_{CO_2}^{bulk}\right]t \quad (24)$$

The model given by Eq. 24 accounts for the effects of the partial pressure of CO_2 and CuO concentration on the reaction itself as well as the limitations due to the diffusion of CuO and CO_2. The first term on the left-hand side of the equation governs the reaction rate during the initial stages of the reaction when the product layer is thin and the diffusion of CuO and CO_2 readily takes place. As time progresses and the product layer grows, the reaction term becomes less influential on the reaction rate as the diffusional rates of CuO and CO_2 become more predominant, making the second term on the left side of Eq. 24 more significant.

Experimental

To determine the validity of Eq. 24, experiments at various particle sizes of $BaCO_3$, partial pressures of CO_2, and concentrations of CuO were conducted over a temperature range of 1,083–1,153 K. Over this range, the only reaction that takes place in air environments is Eq. 1 (Sobolik et al., 1993). For comparison, Eq. 24 was also tested using similar experiments for the reaction

$$4BaCO_3 + Y_2O_3 \rightleftharpoons Y_2Ba_4O_7 + 4CO_2 \quad (25)$$

This reaction has not been studied previously even though some of the 123 HTSC experimental conditions could have led to its progression.

Kinetic measurements were performed in situ, using DXRD, which is based on powder diffractometry and consists of a diffractometer [Co(Kα) radiation] equipped with a position-sensitive detector and a hot stage. To initiate an experiment, fine powder samples (0.03 g, ~ 50 μm thick) were loaded onto a platinum heating strip, which was then enclosed in a chamber so that different gaseous environments could be introduced into the system. The heating strip temperatures were measured and controlled by a thermocouple attached to the heating strip. All of the experiments reported here were conducted under isothermal conditions in a He/O_2 (95%/5%) environment with various CO_2 partial pressures ($0 < P_{CO_2} < 0.3$ kPa).

The differential particle sizes of $BaCO_3$ (> 99.9% pure) were made by initially pressing $BaCO_3$ (344,650 kPa) into pellets that were 10 mm in diameter and 5 mm thick. The pellets were then placed into an alumina crucible and calcined at 1,273 K for 12 h, after which they were ground by mortar and pestle until the resulting particles passed through a 45-μm screen. These particles were then screen separated into the two largest size fractions and analyzed with a scanning electron microscope as well as a Microscan Particle Size Analyzer. Finally, the smallest particle size was obtained by grinding the raw $BaCO_3$ in a ball pestle impact grinder for 10 h. Figure 3 shows the results from the particle-size analysis

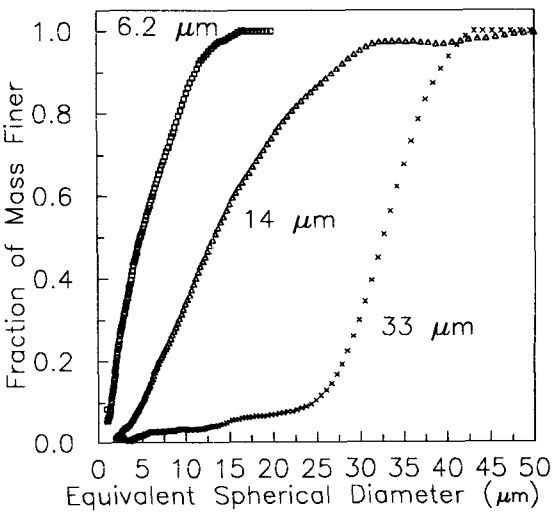

Figure 3. Particle-size mass distribution of the three $BaCO_3$ particle sizes.

where the mass average particle diameters for each of the three different samples were determined to be 6.2 ± 4, 14 ± 8, and 33 ± 7 μm, respectively. The CuO and Y_2O_3 powders had mass average particle sizes of 5.1 ± 3 and 2.6 ± 1 μm, respectively.

Powders of CuO and Y_2O_3 were then mixed with 2 g of the $BaCO_3$ having three distinct particle sizes to achieve a 1:1 and 1:2 cationic ratio for the $BaCO_3$:CuO and Y_2O_3:$BaCO_3$ mixtures, respectively. The six resulting systems were then carefully mixed by mortar and pestle for a period of about 15 min. To study the effects of stoichiometry, only the mixtures incorporating the 6.2 μm $BaCO_3$ particles were investigated, and appropriate quantities of additional CuO and Y_2O_3 were mixed with $BaCO_3$ to obtain the desired concentrations.

In order to obtain quantitative DXRD measurements, an appropriate quantity of an internal standard, $BaZrO_3$, was combined with each of the mixtures to give a sample/standard weight ratio of 5:1 and 2:1 for the $BaCO_3$:CuO and Y_2O_3:$BaCO_3$ systems, respectively. The conversion of each reaction was calculated using the internal standard method (Cullity, 1978) by comparing the ratio of the product and standard peak areas to the same ratio when the reactants were completely consumed.

To conduct an experiment, a sample was introduced into the reaction chamber of the DXRD. A gas of known composition (0.03, 0.10, 0.16, or 0.27 kPa CO_2) was allowed to flow (400 mL/min) through the chamber for a period of 15 min at room temperature to ensure a known reaction environment. The sample was then rapidly heated to the reaction temperature (within a period of 30 s), after which the DXRD recorded the observed reaction. Figure 4 shows a plot of the typical raw data obtained from the DXRD as it monitored a typical Y_2O_3:$BaCO_3$ experiment.

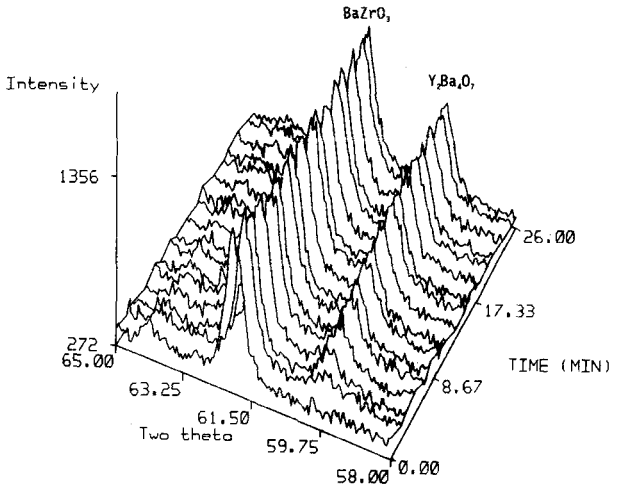

Figure 4. DXRD Spectra: Mixed powders of Y_2O_3 and $BaCO_3$ (6.2 μm $BaCO_3$ at 1,213 K in 0.10 kPa CO_2).

Results and Discussion

Figure 5 shows the results of reacting CuO with the three different particle sizes of $BaCO_3$ at 1,133 K in a He/O_2 environment and also indicates the repeatability of the experiments. It can easily be observed that increasing the particle size of $BaCO_3$ greatly reduced the yield of the reaction. As a general observation, at the end of 25 min, the 14- and 33-μm particles, respectively, achieved only 60 and 30% of the conversion achieved by the 6.2-μm particles. If one assumes that all three particles are identically spherical, the product layer thickness in each instance is very similar ($\sim 0.5 \pm 0.1$ μm), implying that the reaction only proceeds until a specific product thickness is achieved, after which diffusion of either the remaining CuO reactant or the CO_2 produced cannot diffuse to and from the reaction front, respectively.

To apply Eq. 24 to the experimental data, the equilibrium partial pressure of CO_2 must be determined. The equilibrium partial pressure of CO_2 for Eq. 1 was determined analytically (Fjellvåg et al., 1988) to be

$$P^{eq}_{CO_2} = 5.0 \times 10^7 \exp\left(-\frac{20{,}500}{T}\right). \qquad (26)$$

Since the CO_2 equilibrium partial pressure for Eq. 25 was not available in the literature, it was determined experimentally by heating and cooling (3 K/min) $Y_2Ba_4O_7$ in environments of various partial pressures of CO_2 and determining the temperature at which decomposition initiated. Details of these experiments are given elsewhere (Sobolik et al., 1993). Because XRD is only sensitive to species concentrations on the order of a few percent, the measured temperatures are estimated to be accurate to within ± 10 K. Noting this limitation, the effect of temperature on the equilibrium partial pressure was determined to be

$$P^{eq}_{CO_2} = 1.6 \times 10^9 \exp\left(-\frac{26{,}600}{T}\right) \qquad (27)$$

for the Y_2O_3:$BaCO_3$ mixture.

The rate-limiting mechanism(s) for the reaction in Eq. 1 can be evaluated by applying portions of Eq. 24 to the experimental conversion data. For example, if mass transport is fast

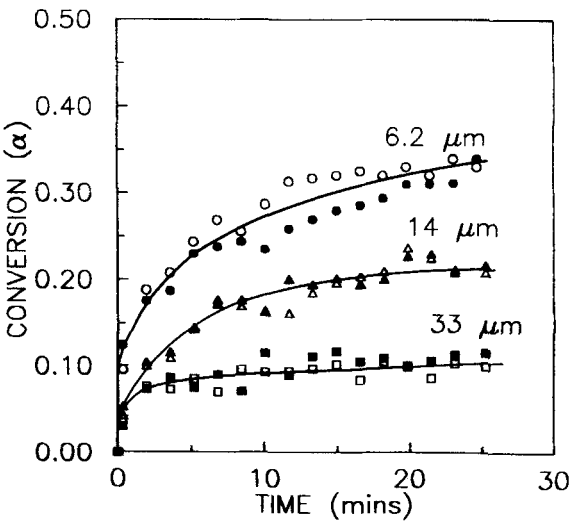

Figure 5. $BaCO_3$:CuO conversion (0.03 kPa CO_2 at 1,133 K).

($D_{CuO} = D_{CO_2} \to \infty$), then a plot of $1-(1-\alpha)^{1/3}$ vs. t should yield a straight line. Similarly, if the kinetics at R_1 are very fast ($k_1' \to \infty$), then either of the two diffusion terms in Eq. 24 may dominate and a plot of $1-3(1-\alpha)^{2/3}+2(1-\alpha)$ vs. t would produce a straight line. In these three situations, the slopes of the lines will be

$$S^r = \frac{k_1' C_{CuO}^{bulk}}{2R\rho_{BaCO_3}}\left[1-\frac{P_{CO_2}^{bulk}}{P_{CO_2}^{eq}}\right] \tag{28}$$

when the surface kinetics control,

$$S_{CO_2}^D = \frac{6D_{CO_2}}{R^2\rho_{BaCO_3}R_gT}\left[1-\frac{P_{CO_2}^{bulk}}{P_{CO_2}^{eq}}\right] \tag{29}$$

when the diffusion of CO_2 controls, and

$$S_{CuO}^D = \frac{6D_{CuO}C_{CuO}^{bulk}}{R^2\rho_{BaCO_3}} \tag{30}$$

when the diffusion of CuO controls the system.

By observing Figure 5 once again, it can be seen that the majority of the conversion takes place as the time reaches approximately 5 min, after which the conversion increases at a much slower rate. This may indicate a change in the mechanism that is controlling the reaction; that is, the reaction is being controlled by the surface kinetics during the first 5 to 6 min when the product layer is thin and, as the product layer grows, the diffusion of CuO and CO_2 through this layer may become the controlling factor. This was substantiated by the fact that neither the diffusion nor the reaction control models were able to fit the data over the entire reaction time. With this in mind, $1-(1-\alpha)^{1/3}$ was applied to the smoothed conversion vs. time data (curves drawn through data, as in Figure 5) for the first 6 min of the reaction and $1-3(1-\alpha)^{2/3}+2(1-\alpha)$ was applied to the data thereafter, and the results are shown in Figure 6. Figure 6 contains the application of the two respective portions of Eq. 24 to the data obtained from the $BaCO_3$ (14 μm) and CuO system reacted at three partial pressures of CO_2 at 1,133 K. First of all, it appeared that the very start of the reaction was most likely controlled by nucleation (Wang et al., 1995), particularly for the smaller particles at the lowest CO_2 pressure. Thus, the data corresponding to the first 1/2 min are given less weight to the straight line shown in Figure 6a. As can be seen, the plots produce reasonably straight lines in both cases, which indicates that the data are consistent with the hypothesized reaction limitations during the times shown. The inability of the diffusion model to fit the data over the entire reaction time can be seen by noting that the straight lines in Figure 6b do not back-extrapolate to the origin. Furthermore, the effect of CO_2 partial pressure on the reaction can also be observed. As shown in Eqs. 28 and 29, increasing the partial pressure of CO_2 should decrease the slope of $1-(1-\alpha)^{1/3}$ vs. time (Eq. 28) when the reaction controls. It should also decrease the slope of $1-3(1-\alpha)^{2/3}+2(1-\alpha)$ vs. time (Eq. 29) when the diffusion of CO_2 controls the reaction rate. In both instances, it can readily be observed (Figure 6) that increasing CO_2 partial pressures resulted in decreased slopes in both time periods, and to the same degree (both slopes decreased by a factor of about 5 when $P_{CO_2}^{bulk}$ was increased from 0.03 to 0.27 kPa), consistent with Eqs. 28 and 29.

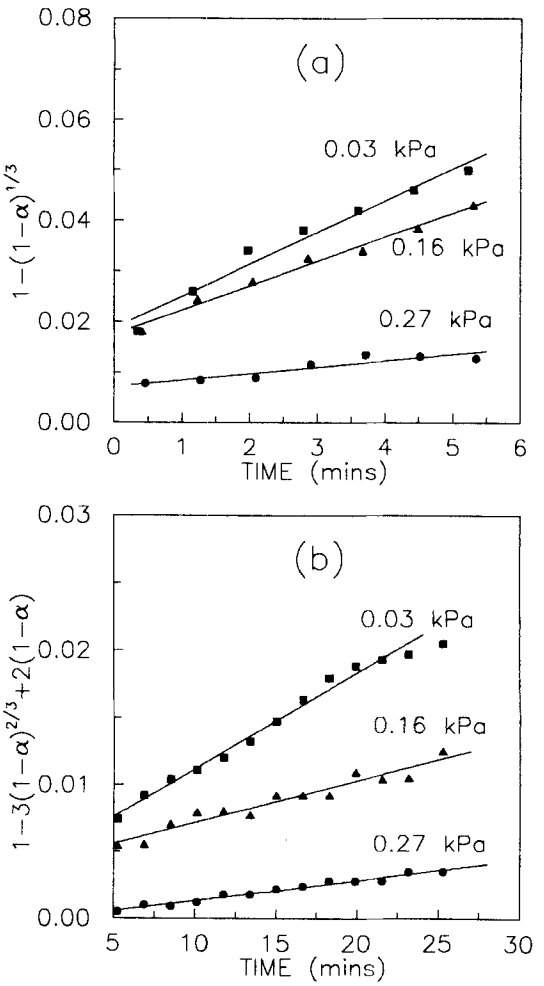

Figure 6. Evaluation of kinetic and diffusion limitations ($BaCO_3$:CuO, 14 μm $BaCO_3$ at 1,133 K).

(a) Reaction controlled. (b) Diffusion controlled.

Similarly, by observing Eqs. 28 and 30, it can be seen that the concentration of CuO should also affect the rate of reaction over both time periods if CuO diffusion is also limiting during the diffusion-controlled portion of the reaction. To determine the effect of CuO on the reaction rates, two different stoichiometric mixtures of $BaCO_3$ (6.2 μm) and CuO (1:1 and 1:4) were heated at 1,083 K in the absence of CO_2, and the resulting conversion vs. time data was manipulated by plotting $1-(1-\alpha)^{1/3}$ and $1-3(1-\alpha)^{2/3}+2(1-\alpha)$ vs. time, as shown in Figure 7. As can be seen, it is quite evident that the concentration of CuO influences the rate of reaction initially (Figure 7a) and throughout the entire progression of the reaction (Figure 7b), as suggested by the increasing slopes with increasing CuO concentrations in both cases.

By observing Figures 6 and 7 it is evident that both CO_2 and CuO affect the system initially when the reaction controls the rate, as well as later on when diffusion appears to be the controlling factor. Because of the limited data during the first 5 min of the reaction, it is possible that the diffusion of

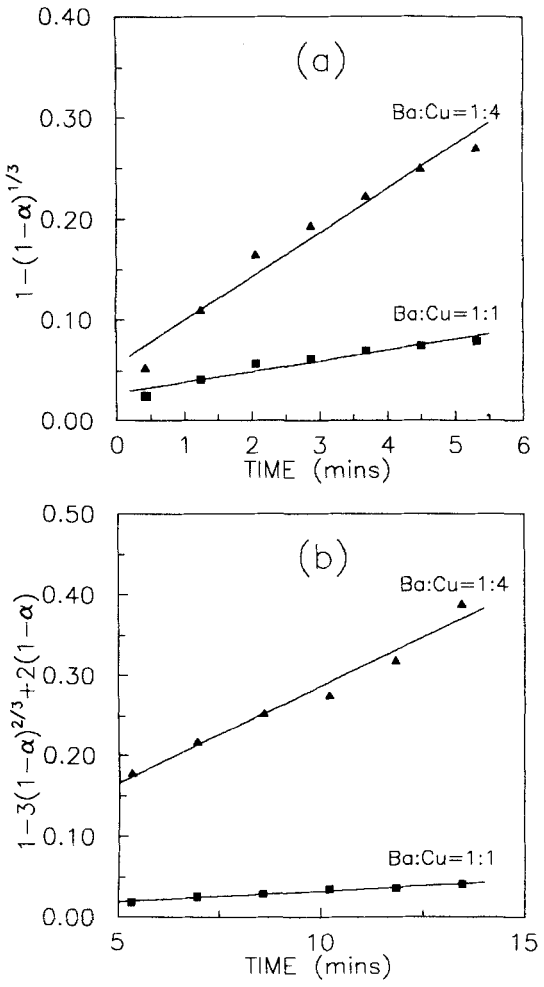

Figure 7. Effect of Ba:Cu ratio (6.2 μm $BaCO_3$ at 1,083 K).

(a) Reaction controlled. (b) Diffusion controlled.

CO_2 and CuO could actually control the system throughout the entirety of the reaction (other than the initial nucleation period). In order to assess the validity of this possibility, experiments were also conducted at different temperatures. With this in mind, a $BaCO_3$ (14 μm):CuO mixture was reacted in 0.03 kPa at four different temperatures ranging from 1,123 to 1,153 K. If the diffusion of CO_2 and CuO were the sole limitations, the reaction rate during the first 5 min would not increase significantly over this small temperature range if their individual diffusivities had a relatively small dependence on temperature. However, this is not likely; for example, Jost (1960) reported that the diffusivity of He in SiO_2 showed a temperature dependence of $D = D_0 \exp(-5{,}600/RT)$. It may also be possible that the CO_2 and CuO diffusivities have a strong dependence on temperature; for example, the diffusivity of O_2 in $YBa_2Cu_3O_{7-x}$ was reported (Hase et al., 1993) to have a temperature dependence of $D = D_0 \exp(-433{,}000/RT)$, in which case the reaction rate would increase exponentially with temperature. It was observed that the rate increased exponentially with temperature during the first 5 min of the reaction as well as at greater times ($5 < t < 30$ min), when diffusion is prevalent, indicating that the diffusivities have a strong dependence on temperature. Since the diffusion portion of Eq. 24 did not fit the data over the entire time range, however, we can conclude that during the initial stages of the reaction when the product layer is thin, diffusion readily takes place and the reaction is controlled by surface kinetics. With this in mind, Eq. 28 was rearranged into

$$k_1' = \frac{2R\rho_{BaCO_3}s^r}{C_{CuO}^{bulk}\left[1-\dfrac{P_{CO_2}^{bulk}}{P_{CO_2}^{eq}}\right]} \tag{31}$$

and an Arrhenius plot of k_1' (Figure 8) yielded

$$k_1' = 5.1\times10^7 \exp\left(-\frac{270{,}000}{RT}\right).$$

With the evidence that both the CuO and CO_2 concentrations affect the rate of reaction, and the fact that the reaction is very dependent on temperature, it can be concluded that all three portions of Eq. 24 are controlling in this system. With this in mind, Eq. 24 was multiplied by R^2/k_1', and the model was applied to the conversion vs. time data after the first minute of the reaction for all of the experiments incorporating the three particle sizes of $BaCO_3$ and various CO_2 partial pressures at 1,133 K. The constants, k_1', D_{CO_2} and D_{CuO} were determined and the value of k_1' was similar to that obtained in Eq. 32, while the values of D_{CO_2} and D_{CuO} were determined to be $9\times10^{-7}\pm5\times10^{-7}$ cm^2/s and $5\times10^{-12}\pm2\times10^{-12}$ cm^2/s, respectively. These values are the same order of magnitude as other diffusing species in solids; that is, 10^{-5}–10^{-16} cm^2/s (Jost, 1960). When these values were then placed back into the model (Eq. 24 multiplied by R^2/k_1'), the right-hand side, $Y_{predicted}$ was plotted vs. the left-hand side Y_{actual}, and the results are shown in Figure 9. With the calculated diffusivities, it is evident that the predicted and actual portions of the model agree satisfactorily. Analysis of the data indicated that the reaction portion of the model was more prevalent in the initial stages of the reaction vs. the

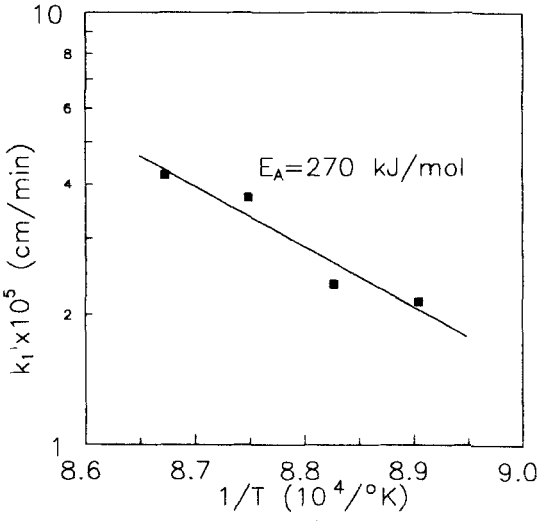

Figure 8. Arrhenius plot for $BaCO_3$:CuO system.

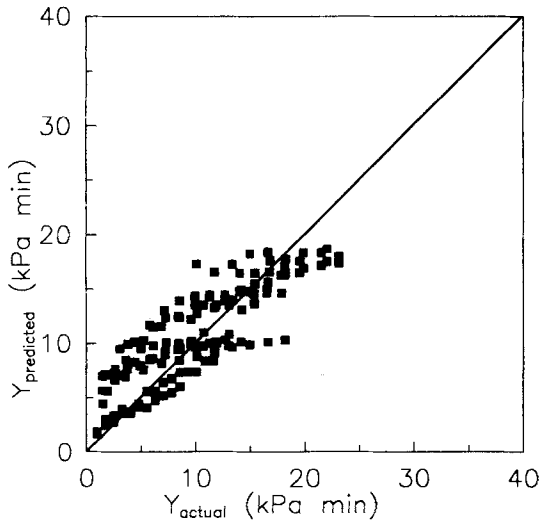

Figure 9. Parity plot: diffusion-limited [$BaCO_3$:CuO, 1,133 K, $D_{CO_2} = 1.9 \times 10^{-7}$ cm²/s, $D_{CuO} = 2.1 \times 10^{-12}$ cm²/s] applied to the $BaCO_3$:CuO mixtures.

latter stages as expected. Furthermore, by analyzing the residuals in Figure 9, the model underestimated the actual system at later times in the reaction. This may be explained by the fact that the reactions slowed down significantly as time progressed to a point where they appeared to stop, in which case the model would not apply. The same type of analysis was also done on the effects of CO_2 partial pressure and particle size. While CO_2 pressure did not have an effect on the residuals, there did appear to be an effect of $BaCO_3$ particle size. Specifically, it was found that the predicted values underestimated the actual values when the small particles were used and it overestimated the actual observations when the large particles were incorporated. Again, this is a consequence of the termination of the reaction when the product layer thickness reaches about 0.5 μm, independent of particle size. That is, the larger particles reach this thickness very shortly (Figure 5), and thus a large fraction of the data points for the larger particles have little or no experimental change and give a false bias to the parity plot. The fact that the residuals for *all* the data scatter equally about the parity line and that kinetics obviously plays a role in the small particles (compare the conversion slopes at 25 min for the small and large particles in Figure 5) points to the necessity of considering both resistances in the model.

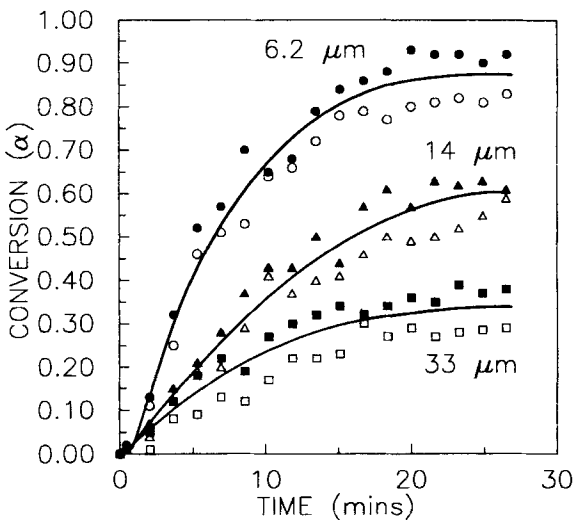

Figure 10. Y_2O_3:$BaCO_3$ conversion (0.10 kPa CO_2 at 1,213 K).

A similar analysis was applied to the data obtained when Y_2O_3 and $BaCO_3$ were reacted at 1,213 K in various environments of CO_2. The conversion vs. time data for the system reacted in 0.10 kPa CO_2 are shown in Figure 10. Again, increasing the particle size from 6.2 to 33 μm reduced the product yield at any given time by an amount similar to that observed in the $BaCO_3$:CuO system.

Although Eq. 25 shows 4 mol of CO_2 produced per mole of $Y_2Ba_4O_7$ produced, there was clear evidence in the XRD data that the reaction actually proceeds in two steps:

$$BaCO_3, \rightleftharpoons BaO + CO_2 \tag{33}$$

$$4BaO + Y_2O_3 \rightarrow Y_2Ba_4O_7 \tag{34}$$

This is based on the fact that BaO XRD reflections were always observed at low CO_2 pressures, and thus the presence of CO_2 in the gas phase served to lower the rate of Eq. 34, which appears to be the rate-limiting step. With this in mind, Eq. 24 can be used to analyze the $BaCO_3$:Y_2O_3 system by simply replacing C_{CuO} and D_{CuO} with $C_{Y_2O_3}$ and $D_{Y_2O_3}$, respectively. When this was done, $1-(1-\alpha)^{1/3}$ and $1-3(1-\alpha)^{2/3}+2(1-\alpha)$ can be plotted vs. time, and straight lines should result if each respective constraint controls the reaction. Figure 11 shows an example of these manipulations on the data of the Y_2O_3 and $BaCO_3$ (14-μm particles) system in three different partial pressures of CO_2, and it is evident that straight lines result. Note that nucleation is not a factor in this system. By observing Figure 11, it can be seen that CO_2 has a significant effect on the rate of the reaction during the initial stages of the reaction, but its effect on the diffusion-controlled portion is much less of a factor than it was in the $BaCO_3$:CuO system (Figure 6b). As in the $BaCO_3$:CuO system, it was found that the system was initially controlled by surface kinetics, followed by diffusion control of both CO_2 and Y_2O_3 at later times. The same exponential temperature dependencies were observed in this system, and the Arrhenius plot yielded

$$k'_{1YBa} = 2.4 \times 10^{13} \exp\left(-\frac{380{,}000}{RT}\right). \tag{35}$$

Finally, the diffusivities of CO_2 and Y_2O_3 were determined to be $3 \times 10^{-6} \pm 6 \times 10^{-7}$ and $4.0 \times 10^{-11} \pm 1.6 \times 10^{-11}$ cm²/s, respectively. Note that the value of D_{CO_2} in the Y_2O_3:$BaCO_3$ system is approximately an order of magnitude greater than that in the $BaCO_3$:CuO system, consistent with the reduced influence of CO_2 on the diffusion-controlled portion of the reaction (Figure 11b).

Conclusions

From the preceding experiments, it can be concluded that Eq. 24 adequately describes the reactions of the $BaCO_3$:CuO

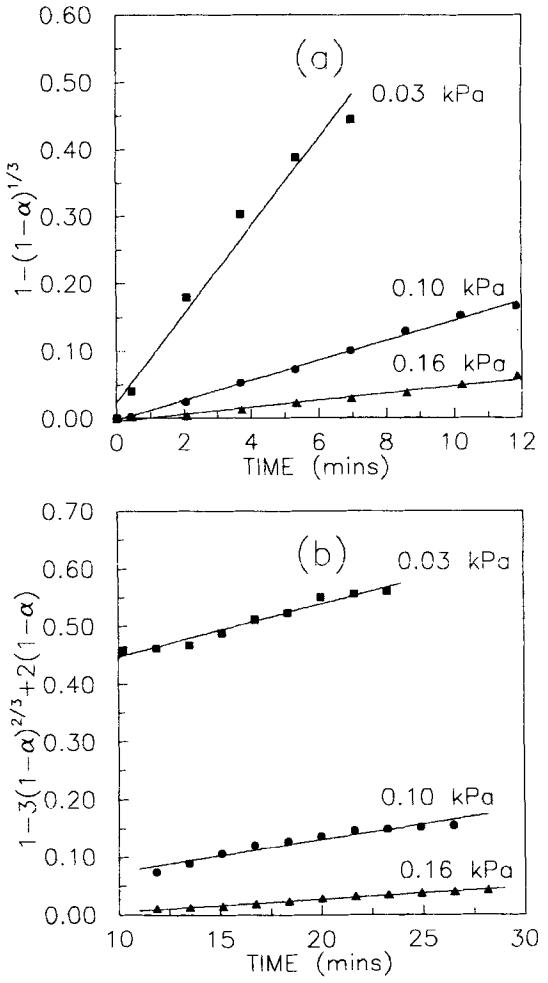

Figure 11. Evaluation of kinetic and diffusion limitations (Y_2O_3:$BaCO_3$, 14 μm $BaCO_3$ at 1,123 K).

(a) Reaction controlled. (b) Diffusion controlled.

and Y_2O_3:$BaCO_3$ systems. The effects of changing the particle size of $BaCO_3$ and the surrounding partial pressure of CO_2 were readily observed when the model was applied to the conversion vs. time data. In both cases, when the particle size of $BaCO_3$ as well as the partial pressure of CO_2 was increased, the rate of reaction decreased. Since neither the diffusion nor the reaction portions of the model were capable of fitting the data over the entire reaction time, both systems appeared to be controlled initially by the reaction until the product layer thickness became substantial, after which the diffusion of the migrating species became the controlling factor. This is true in all three of the particle sizes studied; it is just that the cessation of reaction (at ~ 0.5 μm) occurs sooner in the large particles than in the smaller particles. It has also been shown that changing the concentration of both CO_2 and CuO had an effect on the rates throughout the reaction. It does not appear that either of these two species is more dominant and, since the data are adequately described by Eq. 24, it is likely that both are equally important.

In relating these findings to the processing of the 123 HTSC, it becomes more understandable why the intermediate $BaCuO_2$ is present while $Y_2Ba_4O_7$ is not: $Y_2Ba_4O_7$ requires much more energy to form than the $BaCuO_2$. Furthermore, it has been shown that the rate of formation of both $BaCuO_2$ and $Y_2Ba_4O_7$ is dependent on the diffusion of CO_2 away from the reaction front. As the reactions proceed, these localized CO_2 concentrations may indeed inhibit complete reactions that ultimately lead to other reactions, which form undesirable phases in the 123 final product. In summary, the reactions between $BaCO_3$ and the metallic oxides of CuO and Y_2O_3 have been observed using DXRD and appear to follow the "shrinking core" behavior that is adequately modeled by Eq. 24 to give the dependence of the reaction rate on CO_2 pressure and the $BaCO_3$ particle size.

Notation

k_{BaCO_3} = proportionality constant, $a_{BaCO_3}/4\pi r^2$, cm^{-2}
k_{BaCuO_2} = proportionality constant, $a_{BaCuO_2}/4\pi r^2$, cm^{-2}
k_{CuO} = proportionality constant, a_{CuO}/C_{CuO}, cm^3/mol
k'_1 = combined constant for $BaCO_3$:Y_2O_3 system, cm/min
k'_{1YBa} = combined constant for Y_2O_3:$BaCO_3$ system, cm/min
K_{eq} = equilibrium constant, kPa
N_i = moles of species i, mol
r = instantaneous radius of particle, cm
R = initial radius of particle, cm
t_{CuO} = time necessary for the reaction when mass transport of CuO dominates, min
t_{CO_2} = time necessary for the reaction when mass transport of CO_2 dominates, min
ρ_{BaCO_3} = molar density of $BaCO_3$, mol/cm^3

Literature Cited

Campbell, J. H., "The Kinetics of Decomposition of Colorado Oil Shale: II. Carbonate Minerals," Lawrence Livermore Lab., Univ. of California, Livermore, CA (1978).

Cooper, E. A., A. K. Gangopadhyay, T. O. Mason, and U. Balachandran, "CO_2 Decomposition Kinetics of $YBa_2Cu_3O_{7-x}$ Via *In Situ* Electrical Conductivity Measurements," *J. Mat. Res.*, **6**, 1393 (1991).

Cullity, B. D., *Elements of X-Ray Diffraction*, Addison-Wesley, Reading, MA, p. 415 (1978).

Fjellvåg, H., P. Karen, A. Kjekshus, P. Kofstad, and T. Norby, "Carbonization of $YBa_2Cu_3O_{6+x}$," *Acta Chem. Scand. A*, **42**, 178 (1988).

Gadalla, A. M., and T. Hegg, "Kinetics and Reaction Mechanisms for Formation and Decomposition of $Ba_2YCu_3O_x$," *Thermochim. Acta*, **145**, 149 (1989).

Gao, Y., K. L. Merkel, C. Zhang, U. Balachandran, and R. B. Poeppel, "Decomposition of $YBa_2Cu_3O_{7-x}$ During Annealing in CO_2/O_2 Mixtures," *J. Mat. Res.*, **5**, 1363 (1990).

Hase, T., R. Kita, K. Kawaguchi, T. Koga, and T. Morishita, "Synthesis of $YBa_2Cu_3O_{7-x}$ Thin Films by Three-Stage Oxidation Process From Metallic Y-Ba-Cu Precursors," *J. Mater. Res.*, **8**, 1220 (1993).

Huang, T. W., M. P. Hung, T. S. Chin, P. C. Yao, C. L. Ong, and S. E. Hsu, "The Kinetics of Solid State Formation of the $YBa_2Cu_3O_{6-5-x}$ Phase," *Superconductivity and Applications*, P. T. Wu, H. C. Ku, W. H. Lee, and R. S. Liu, eds., World Scientific, Singapore, p. 319 (1989).

Jiang, X. P., J. S. Zhang, J. G. Huang, G. W. Qiao, Z. Q. Hu, and C. X. Shi, "Study on Solid State Reaction Process of the $YBa_2Cu_3O_{7-x}$ Compound," *Mat. Lett*, **7**, 250 (1988).

Jost, W., *Diffusion in Solids, Liquids and Gases*, Academic Press, New York, p. 215 (1960).

Levenspiel, O., *Chemical Reaction Engineering*, Wiley, New York, p. 371 (1972).

Ruckenstein, E., and N. L. Wu, "A Two-Step Calcination Method for Preparing $YBa_2Cu_3O_{7-x}$ Powders," *Mat. Lett.*, **7**, 165 (1988).

Ruckenstein, E., S. Narain, and N. L. Wu, "Reaction Pathways for the Formation of the $YBa_2Cu_3O_{7-x}$ Compound," *J. Mat. Res.*, **4** 267 (1989).

Selvaduray, G., C. Zhang, U. Balachandran, Y. Gao, K. L. Merkle, H. Shi, and R. B. Poeppel, "Effect of CO_2 on the Processing of Y-Ba-Cu-O Superconductors," *J. Mat. Res.*, 7, 283 (1992).

Sobolik, J. L., H. Wang, and W. J. Thomson, "The Effect of Particle Size and Oxygen on the Binary Reactions Leading to the Y-Ba-Cu HTSC," *J. Amer. Ceram. Soc.*, 77, 2738 (1994).

Tamhankar, S. S., and L. K. Doraiswamy, "Analysis of Solid-Solid Reactions: a Review," *AIChE J.*, **25**, 561 (1979).

Thomson, W. J., "Dynamic X-ray Diffraction: A Technique for Following Solid-State Reactions," *Ceramic Transactions*, Vol. 5, *Advanced Characterization Techniques for Ceramics*, W. S. Young, G. L. McVay, and G. E. Pike, eds., American Ceramic Society, Westerville, OH, p. 131 (1989).

Thomson, W. J., H. Wang, D. B. Parkman, D. X. Li, M. Strasik, T. S. Luhman, H. Chan, I. A. Aksay, "Reaction Sequencing During Processing of the 123 Superconductor," *J. Amer. Ceram. Soc.*, **72**(10), 1977 (1989).

Wang, H., and W. J. Thomson, "Binary Kinetics in the Y-Ba-Cu System: 2. Nanosized Precursors," *AIChE J*, **41**(6), (1995).

Wu, N. L., T. C. Wei, S. Y. Hou, and S. Y. Wong, "Kinetic Study and Modeling of the Solid-State Reaction $Y_2BaCuO_5 + 3BaCuO_2 + 2CuO \rightarrow 2YBa_2Cu_3O_{6.5-x} + xO_2$," *J. Mat. Res.*, **5**, 2056 (1990).

Manuscript received Jan. 18, 1994, and revision received Oct. 17, 1994.